J|A|C|S
ARTICLES
Published on Web 02/14/2003

Single Crystalline Commensurate Metallic Assemblages of π-slabs and CdI_2-Type Layers: Synthesis and Properties of β-(EDT-TTF-I_2)$_2$[$Pb_{5/6}\square_{1/6}I_2$]$_3$ and β-(EDT-TTF-I_2)$_2$[$Pb_{2/3+x}Ag_{1/3-2x}\square_xI_2$]$_3$, $x = 0.05$

Thomas Devic,[†,‡] Michel Evain,[§] Yves Moëlo,[§] Enric Canadell,[||] Pascale Auban-Senzier,[⊥] Marc Fourmigué,[†,‡] and Patrick Batail*[,†,‡]

Contribution from the Laboratoire de Chimie Inorganique, Matériaux et Interfaces, CNRS FRE 2447, Université d'Angers, Bâtiment K, 2 Boulevard Lavoisier, 49045 Angers, France, the CNRS FRE 2068 and UMR 6502 at the Institut des Matériaux Jean Rouxel, 2 rue de la Houssinière, 44322 Nantes, France, the Institut de Ciència de Materials de Barcelona (CSIC), Campus de la U.A.B., 08193 Bellaterra, Spain, and the Laboratoire de Physique des Solides, Université de Paris-Sud, 91405 Orsay, France

Received October 22, 2002; E-mail: patrick.batail@univ-angers.fr

Abstract: The ability of I···I van der Waals interactions to direct the self-assembly of slabs of the radical cation of ethylenedithio-1,2-diiodo-tetrathiafulvalene, EDT-TTF-I_2, and polymeric lead iodide covalent anionic layers is demonstrated by the synthesis of single crystals of β-(EDT-TTF-I_2)$_2^{\bullet+}$[($Pb_{5/6}\square_{1/6}I_2$)$^{1/3-}$]$_3$, triclinic, P-1, $a = 7.7818(8)$, $b = 7.9760(8)$, $c = 19.9668(2)$ Å, $\alpha = 82.409(12)$, $\beta = 85.964(12)$, $\gamma = 61.621(11)°$, V = 1080.76(19) Å^3, $R1$, w$R2 = 0.0459$, 0.0947; and β-(EDT-TTF-I_2)$_2^{\bullet+}$[($Pb_{2/3+x}Ag_{1/3-2x}\square_x I_2$)$^{1/3-}$]$_3$, $x \approx 0.05$, triclinic, P-1, $a = 7.7744(8)$, $b = 7.9193(8)$, $c = 19.834(2)$ Å, $\alpha = 87.189(12)$, $\beta = 83.534(12)$, $\gamma = 61.602(11)°$, V = 1067.4(2) Å^3, $R1$, w$R2 = 0.0508$, 0.0997. The state-of-the-art, combined microprobe and structural analysis of the metal site vacancies and occupancies patterns reveal a commensurate organic−inorganic interface and point out the importance of halogen···halogen van der Waals interactions to future studies aiming at directing interface topologies. The electronic structure, room-temperature metallic character and metal−insulator transition at ca. 70 K of the two-dimensional organic slabs are retained upon alloying of the inorganic sublattice with monocations. The room-temperature conductivity of the metallic lead−silver alloy is 2 orders of magnitude larger than that of β-(EDT-TTF-I_2)$_2^{\bullet+}$[($Pb_{5/6}\square_{1/6}I_2$)$^{1/3-}$]$_3$. This calls for the study of materials with diverse alloying patterns with metal cations of different nature and charge.

Introduction

The manipulation of weak noncovalent intermolecular interactions—here I···I van der Waals interactions—which direct the self-assembly dynamics of anisotropic, eventually charged or covalent, extended molecular motifs during nucleation process at the crystal−solution interface to form solids ordered at large length scales is a topic of great current interest relevant to many diverse fields of molecular sciences.[1−6] A valuable, rational-design approach in materials science has been to try and reconstruct solids upon intercalation of ions or molecules within exfoliated mineral sheets.[7] The expectation that they would fit and recombine into ordered composite interfaces is rarely satisfied. By and large, long-range ordering of the latter at the large length scales typical of macroscopic single crystals is not achieved because of the lack of synthesis design for the concomitant reconstruction of an extended covalent motif in solution.[8] In this paper, we report on single crystals of two such solids and demonstrate successful net intercalation: metallic, iodine-functionalized radical cation β-nets[9] are found to be exacted by extended, ordered hexagonal covalent PbI_2 polymer sheets, with the CdI_2 structure type.

† CNRS FRE 2447, Angers.
‡ CNRS FRE 2068, Nantes.
§ CNRS UMR 6502, Nantes.
|| CSIC, Bellaterra.
⊥ Laboratoire de Physique des Solides, Orsay.

(1) (a) Guloy, A. M.; Tang, Z.; Miranda, P. B.; Srdanov, V. I. *Adv. Mater.* **2001**, *13*, 833−837. (b) Tang, Z.; Guloy, A. M. *J. Am. Chem. Soc.* **1999**, *121*, 452−453.
(2) Cariati, E.; Ugo, R.; Cariati, F.; Roberto, D.; Masciocchi, N.; Galli, S.; Sironi, A. *Adv. Mater.* **2001**, *13*, 1665−1668.
(3) Umbach, E.; Glöckler, K.; Sokolowski, M. *Surf. Sci.* **1998**, *402*−*404*, 20−31.
(4) Deluzet, A.; Rousseau, R.; Guilbaud, C.; Granger, I.; Boubekeur, K.; Batail, P.; Canadell, E.; Auban-Senzier, P.; Jérôme, D. *Chem. Eur. J.* **2002**, *8*, 3884−3900.
(5) Petruska, M. A.; Watson, B. C.; Meisel, M. W.; Talham, D. R. *Chem. Mater.* **2002**, *14*, 2011−2019.
(6) Wu, C.-G.; Degroot, D. C.; Marcy, H. O.; Schindler, J. L.; Kannewurf, C. R.; Bakas, T.; Papaefthymiou, V.; Hirpo, W.; Yesinowski, J. P.; Liu, Y.-J.; Kanatzidis, M.-G. *J. Am. Chem. Soc.* **1995**, *117*, 9229−9242.
(7) (a) Rao, C. N. R.; Gopalakrishnan, J. In *New Directions in Solid State Chemistry*, 2nd ed.; Cambridge University Press: Cambridge, 1997. (b) Gopalakrishnan, J. *Chem. Mater.* **1995**, *7*, 1265−1275. (c) Rouxel, J.; Tournoux, M. *Solid State Ionics* **1996**, *84*, 141−149.
(8) See, for example: (a) Schaak, R. E.; Mallouk, T. E. *Chem. Mater.* **2002**, *14*, 1455−1471. (b) Uma, S.; Raju, A. R.; Gopalakrishnan J. *J. Mater. Chem.* **1993**, *3*, 709−713 and references therein.
(9) Mori, T. *Bull. Chem. Soc. Jpn.* **1998**, *71*, 2509−2526.

Scheme 1

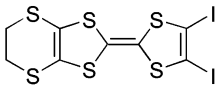

EDT-TTF-I_2, $E^1_{1/2} = 0.60$ V, $E^2_{1/2} = 0.89$ V vs SCE in benzonitrile.

Our synthetic approach of the design of the organic−inorganic interface in the title series focuses on halogen···halogen van der Waals interactions. They play a major role at the mesoscopic length scale in the dynamics of small confining systems in colloidal science and supramolecular chemistry as well as in issues regarding adsorption processes nearby a solid surface, especially since van der Waals interactions are sensitive to surface geometry and curvature.[3,10−11] In addition, we choose to bridge toward earlier approaches of the design of organic metals with two-dimensional polymeric metal halide anion networks by the groups of Shibaeva−Yagubskii, Geiser, Zhu, and Kobayashi, typically engaging nonfunctionalized radical cations, as exemplified by $(BEDT\text{-}TTF)_2Cu_5I_6$ (BEDT-TTF = bis(ethylenedithio)tetrathiafulvalene),[12] $(BEDT\text{-}TTF)_6(PbBr_3)_3\cdot PhCl\cdot Me_2CO$,[13] $(BEDT\text{-}TTF)Ag_xBr_3$,[14] $(TTM\text{-}TTF)_3Cu_2Cl_x$ (TTM-TTF = tetrakis(methyl)tetrathiafulvalene),[15] and $(BETS)_2Cu_5I_6$ (BETS = bis(ethylenedithio)tetraselenafulvalene),[16] on one hand,[17] and the complementary perspective provided by the work of Mitzi group on alkylammonium salts of metal halide layered hybrid perovskites[18] of Guloy group on $DAMS^+$ salts of $[PbI_3^-]_\infty$ chains ($DAMS^+$ = *trans*-4-(4-dimethylaminostyryl)-1-methylpyridinium)[1a] or of Cariati and Sironi groups on the series $[DAMS^+]_m[M_nI_{n+m}]$ (M = Cu, Ag).[2]

Finally, the present prototypes of two precise substructures of an ordered, lacunar phase or lead−silver alloy are unprecedented and offer an entry to further systematic studies of their structure−property relationship which were precluded by experimental difficulties inherent to studying highly disordered powder solids since no single crystals were available.[19]

Experimental Section

Electrocrystallization. A two-compartment cell equipped with platinum electrodes (l = 2 cm, Ø = 1 mm) and kept at 20 °C was filled with ethylenedithio-1,2-diiodo-tetrathiafulvalene, EDT-TTF-I_2 (5 mg), prepared as described previously (Scheme 1),[20] dissolved in freshly distilled acetonitrile (10 mL) together with PbI_2 (50 mg) and NaI (25 mg) for **1**, and PbI_2 (80 mg), NaI (45 mg), and AgI (20 mg) for **2**, which serve as electrolyte.

Table 1. Crystallographic Data and Structure Refinement for **1** and **2**

identification	**1**	**2**
empirical formula	$C_8H_4I_5Pb_{1.25}S_6$	$C_8H_4Ag_{0.25}I_5Pb_{1.2}S_6$
formula weight	1186	1111.3
crystal system	triclinic	triclinic
space group	P-1	P-1
unit cell dimensions		
a (Å)	7.7818(8)	7.7744(8)
b (Å)	7.9760(8)	7.9193(8)
c (Å)	19.9668(2)	19.834(2)
α (°)	82.409(12)	87.189(12)
β (°)	85.964(12)	83.534(12)
γ (°)	61.621(11)	61.602(11)
V (Å^3)	1080.76(19)	1067.4(2)
independent reflections	3894	9233
S	1.55	1.70
final R indices [$I > 2\sigma(I)$]		
$R1^a$, $wR2^b$	0.0459, 0.0947	0.0508, 0.0997

^{a} $R1 = \Sigma(||Fo| - |Fc||)/\Sigma|Fo|$. ^{b} $wR2 = [\Sigma(w(Fo^2 - Fc^2)^2)/\Sigma(Fo^2)^2]^{1/2}$, and S = goodness-of-fit on $F^2 = [\Sigma(w(Fo^2 - Fc^2)^{2)}/(n - p)]^{1/2}$, where n is the number of reflections and p is the number of parameters refined.

Oxidation at low constant current (0.1 μA) afforded after 20 days single crystals too small for X-ray diffraction. Larger crystals appropriate for crystal structure determination and transport measurements were obtained by rhythmic reversal of the current flow (1 μA, oxidation for 0.7 s, reduction for 0.3 s), as described previously by Hünig et al.[21] The crystals were collected on the anode and washed with acetonitrile. On any given batch, crystals of a homogeneous single phase appear either black and shiny for the thicker single crystals or brown-orange and shiny for the thinner ones.

Crystal Structures. β-$(EDT\text{-}TTF\text{-}I_2)_2^{\cdot+}[(Pb_{5/6}\square_{1/6}I_2)^{1/3-}]_3$ 1. Data collection was carried out on a Stoe-IPDS diffractometer operating at 293 K, with graphite-monochromated Mo−$KL_{2,3}$ radiation (λ = 0.71069 Å). After a Lorentz-polarization adjustment with the STOE software,[22] the intensities were corrected for absorption (Gaussian analytical method) using JANA2000.[23] The structure was partially solved using Patterson method (SHELXS)[24] and all subsequent calculations were carried out with JANA2000. As anticipated, PbI_2 layers were identified, although Pb occupancy had to be released and refined in the final stage to yield a stoichiometry close to $Pb_{5/6}\square_{1/6}I_2$ (site occupancies: Pb1 (inversion center), 0.874(4); Pb2 (general position), 0.888(3)). The identification of the EDT-TTF-I_2 molecule was far more complicated. If the iodine and sulfur atoms were easily located, the lighter carbon atoms could not be refined at meaningful positions. In addition, strong residues remained unexplained and atomic displacement parameters had nonphysical values for some atoms. A thorough investigation of the difference Fourier strongest peaks (positive and negative) gave a hint for a possible disorder. A rigid body was then introduced, providing for three partially overlapping, identical molecules shifted by ca. (1/3, 1/ 3, 0). With proper constraints for the occupancies (one coherent set of molecules per slab), anisotropic displacement parameters for all atoms but C7 and C8 and a common, refined isotropic displacement parameter for H atoms, the residual R value converged to 0.0459 for 2420 observed reflections and 195 parameters. Notice that it was not possible to refine a secondary extinction coefficient. Details of data collection and structure refinement are given in Table 1. The full set of crystallographic data is available in the Supporting Information (Table S1).

(10) Blum, Z.; Hyde, S. T.; Ninham, B. W. *J. Phys. Chem.* **1993**, *97*, 661−665.
(11) Forrest, S. R. *Chem. Rev.* **1997**, *97*, 1793−1896.
(12) (a) Buravov, L. I.; Zvarykina, A. V.; Kartsovnik, M. V.; Kushch, N. D.; Laukhin, V. N.; Lobkovskaya, R. M.; Merzhanov, V. A.; Fedutin, L. N.; Shibaeva, R. P.; Yagubskii, E. B. *Sov. Phys. JETP* **1987**, *65* (2), 336−338. (b) Shibaeva, R. P.; Lobkovskaya, R. M. *Sov. Phys. Crystallogr.* **1988**, *33* (2), 241−243.
(13) (a) Zhilyaeva, E. I.; Lyubovskaya, R. N.; Gritsenko, V. V.; Dyachenko, O. A.; Yudanova, E. I.; Lyubovskii, R. B. *Synth. Met.* **1995**, *70*, 1183−1184. (b) Dyachenko, O. A.; Gritsenko, V. V.; Shilov, G. V.; Zhilyaeva, E. I.; Lyubovskaya, R. N. *Russ. Chem. Bull.* **1995**, *44*, 883−889.
(14) Geiser, U.; Wang, H. H.; Rust, P. R.; Tonge, L. M.; Williams, J. M. *Mol. Cryst. Liq. Cryst.* **1990**, *181*, 117−124.
(15) Liu, S.-G.; Wu, P.-J.; Zhu, D. B. *Synth. Met.* **1997**, *86*, 2031−2032.
(16) Kushch, N. D.; Dyachenko, O. A.; Gritsenko, V. V.; Buravov, L. I.; Tkacheva, V. A.; Yagubskii, E. B.; Kaplunov, M. G.; Golubev, E. V.; Togonidze, T. G.; Kobayashi, A.; Kobayashi, H. *J. Mater. Chem.* **1999**, *9*, 687−691.
(17) Note that preliminary data for a phase-formulated $(BEDT\text{-}TTF)PbI_3$ have been reported: Papavasilliou, G. C.; Patsis, A. P.; Lagouvardos, D. J.; Koutselas, I. B. *Synth. Met.* **1993**, *55*−*57*, 3889−3894.
(18) (a) Mitzi, D. B. *Prog. Inorg. Chem.* **1999**, *48*, 1−121. (b) Mitzi, D. B. *J. Chem. Soc., Dalton Trans.* **2001**, 1−12 and references therein.
(19) Hull, S.; Keen, D. A.; Berastegui, P. *Solid State Ionics* **2002**, *147*, 97−106.
(20) Domercq, B.; Devic, T.; Fourmigué, M.; Auban-Senzier, P.; Canadell, E. *J. Mater. Chem.* **2001**, *11*, 1570−1575.
(21) Hünig, S.; Kemmer, M.; Meixner, H.; Sinzger, K.; Wenner, H.; Bauer, T.; Tillmans, E.; Lux, F. R.; Hollstein, M.; Gross, H.-G.; Langohr, U.; Werner, H.-P.; von Schütz, J. U.; Wolf, H.-C. *Eur. J. Inorg. Chem.* **1999**, 899−916.
(22) STOE Software; Stoe & Cie. Gmbh: Darmstadt, Germany, 1996.
(23) Petricek, V.; Dusek, M. *JANA2000, A Crystallographic Computing System*, Institute of Physics, Academy of Sciences of the Czech Republic: Prague, 2000.
(24) Sheldrick, G. M. *SHELXS-86, Program for crystal structure resolution;* University of Göttingen: Göttingen, Germany, 1986.

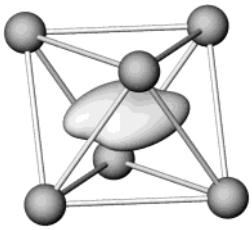

Figure 1. Three-dimensional representation of a joint probability density isosurface for Pb2/Ag2. Iodine atoms are represented as spheres of arbitrary size.

***β*-(EDT-TTF-I$_2$)$_2$$^{\bullet+}$[(Pb$_{2/3+x}Ag_{1/3-2x}$□$_xI_2$)$^{1/3-}$]$_3$ 2.** Two data collections were carried out. A first intensity collection was realized on the Stoe IPDS diffractometer ($\sin(\theta)/\lambda \leq 0.65$ Å^{-1}) and a second on a Nonius CAD-4F diffractometer to collect reflections at higher $\sin(\theta)/\lambda$ (up to 0.8 Å^{-1}). Usual corrections were applied (vide supra) and the two sets were scaled according to 690 common reflections with $I/\sigma(I) > 10$ (scale factors 1.0/0.0589(10)). The structure was once again solved using Patterson method (SHELXS). This time, difficulties came on the mixed Pb/Ag layers and no disorder appeared on the EDT-TTF-I$_2$ molecular part. The two octahedral independent sites of the Pb$_x$Ag$_y$I$_2$ layers had a different behavior, one site being fully occupied by Pb and the other site ca. equally by Pb and Ag. Since Pb (II) is usually found at the center of the octahedron but Ag (I) is not (being displaced toward some of the faces[25]), a particular electron density distribution occurs. The electron density of the site with mixed occupancy could be either modeled by a Gram−Charlier nonharmonic development of the Debye−Waller factor[26] or a splitting of atoms, the model giving smaller correlation being more appropriate. Both models have been tried and the splitting proved to be more appropriate. The joint probability density function of Ag2 and Pb2 is presented in Figure 1. Without constraints for the Ag2 and Pb2 occupancies, anisotropic displacement parameters for all atoms, no H atoms and no secondary extinction, the residual *R* value converged to 0.0508 for 3701 observed reflections and 198 parameters. Details of data collection and structure refinement are given in Table 1. The full set of crystallographic data is available in the Supporting Information (Table S2).

Electron Probe Microanalysis (EPMA). Electron probe microanalysis (EPMA) was performed with a CAMECA SX 50 apparatus equipped with wavelength dispersive spectrometers (common IFREMER-CNRS-Université de Bretagne Occidentale Laboratory, Brest, France). Operating conditions were as follows: accelerating voltage 15 kV; beam current 15 nA; counting time for one spot analysis 5 s; standards (element, emission line): PbS (Pb, *M*α), synthetic $Pb_2SbS_2I_3$ (I, *L*α), FeS_2 (S, *K*α), pure Ag (Ag, *L*α). Several crystals were included in epoxy resin and prepared as polished sections. Eleven and seven spot analyses were collected for **1** and **2**, respectively, with a defocused electron beam (diameter 20 μm for **1** and 10 μm for **2**). Moreover, it was necessary to scan the crystal surface during acquisition time to prevent any damage under the electron beam. Analytical data are given in the Supporting Information.

Band Structure Calculations. The tight-binding band structure calculations and $\beta_{HOMO-HOMO}$ interaction energies were based upon the effective one-electron Hamiltonian of the extended Hückel method.[27] The off-diagonal matrix elements of the Hamiltonian were calculated according to the modified Wolfsberg−Helmholz formula.[28] All valence electrons were explicitly taken into account in the calculations and the basis set consisted of double-ζ Slater-type orbitals for C, S, and I and single-ζ Slater-type orbitals for H. The exponents, contraction coefficients, and atomic parameters for C, S, I, and H were taken from previous work.[20]

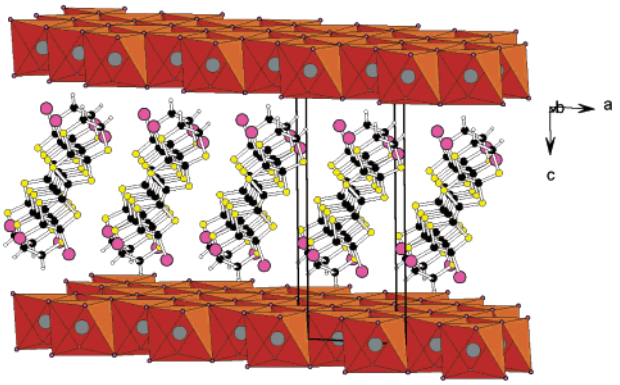

Figure 2. A perspective view of the structure common to the two phases. Note the typical topology of the edge-sharing metal iodide octahedral slabs.

Electronic Conductivity. The resistivity of both materials was measured from 295 down to 4.2 K at ambient pressure on single crystals using the four probe low-frequency lock-in technique with measuring currents lower than 10 μA. To minimize the resistance of the contacts, four gold pads have been evaporated along the largest face and on both sides of the plateletlike crystals.

Magnetic Measurements. The ESR spectra was recorded on a polycrystalline sample at room temperature on an X-band (9.86 GHz) Bruker spectrometer. Magnetic susceptibility measurements were performed on a polycrystalline sample (23 mg) of **1** on a Quantum Design MPMS-5 SQUID magnetometer in the temperature range 2.5−350 K at 10 kOe. The data were corrected for the sample holder and for the diamagnetic contribution calculated from Pascal constants.

Results and Discussion

The two phases, formulated *β*-(EDT-TTF-I$_2$)$_2$$^{\bullet+}$[(Pb$_{5/6}$□$_{1/6}I_2$)$^{1/3-}$]$_3$ and *β*-(EDT-TTF-I$_2$)$_2$$^{\bullet+}$[(Pb$_{2/3+x}Ag_{1/3-2x}$□$_xI_2$)$^{1/3-}$]$_3$, $x \approx 0.05$, by a combination of crystal structure resolution data and microprobe analysis results (vide infra), have a common triclinic layered structure shown in Figure 2 which exemplifies how single *β*-EDT-TTF-I$_2$ layers intercalate single Pb$_x$Ag$_y$I$_2$ slabs.

In both phases, the asymmetric unit consists of one EDT-TTF-I$_2$, three iodides, and one metal atom in general position, and a second metal atom on the inversion center. Edge-sharing PbI$_6$ octahedra form a bidimensional inorganic polymer with the CdI$_2$ structure type. Remarkably, these layers typically have the structure of a discrete slab in neutral, layered hexagonal PbI$_2$.[29] Hence, the resolution of the ordered structures of the single crystals of **1** and **2** provides the first and long awaited examples of crystal structures of PbI$_2$ intercalation compounds. The closest approach was provided recently by Guloy et al. in their description of molecular $[Pb_2I_6^{2-}]_\infty$ double chains of edge-sharing octahedra, given as a direct structural parentage to the extended layered phase PbI$_2$.[30] Indeed, there have been numerous attempts at intercalating a variety of neutral molecules such as pyridine, aniline, hydrazine, and organic amines[31−33] into PbI$_2$

(25) Gaudin, E.; Boucher, F.; Evain, M. *J. Solid State Chem.* **2001**, *160*, 212−221.
(26) Johnson, C. K.; Levy, H. A. In *International Tables for X-ray Crystallography*; Ibers, J. A., Hamilton, W. C., Eds.; Kynoch Press: Birmingham, 1974; Vol. IV, pp 311−336.
(27) Whangbo, M.-H.; Hoffmann, H. *J. Am. Chem. Soc.* **1978**, *100*, 6093−6098.
(28) Ammeter, J.; Bürgi, H.-B.; Thibeault, J.; Hoffmann, R. *J. Am. Chem. Soc.* **1978**, *100*, 3686−3692.
(29) Trigunayat, G. C. *Solid State Ionics* **1991**, *48*, 3−70.
(30) Chakravarthy, V.; Guloy, A. M. *J. Chem. Soc., Chem Commun.* **1997**, 697−698.
(31) (a) Koshkin, V. M.; Kukol, V. V.; Milner, A. P.; Zabrodskii, Y. R.; Katrunov, K. A. *Sov. Phys. Solid State* **1977**, *19*, 939−941. (b) Gurina, G. I.; Evtushenko, V. D.; Gritskaa, N. A.; Koshin, V. M. *Russ. J. Inorg. Chem.* **1986**, *31*, 469−471.

which only yielded crystalline powders for which only a schematic description of the intercalated structure was possible.

***β*-(EDT-TTF-I$_2$)$_2$$^{\bullet+}$[(Pb$_{5/6}$□$_{1/6}I_2$)$^{1/3-}$]$_3$ 1.** The successful growth of single crystals by electro-oxidation of the neutral molecular precursor was a first indication for the presence of an anionic inorganic motif. This was readily confirmed in the course of the structure refinement which provided evidence for equivalent amounts of vacancies (12%) on both lead atom sites. Extensive quantitative electron probe microanalysis (EPMA) was then carried out and yielded a slightly higher vacancy concentration (17%, see Supporting Information), that is, close to an overall 1/6 lead deficiency. The latter ultimately yields the compound formulation, *β*-(EDT-TTF-I$_2$)$_2$$^{\bullet+}$[(Pb$_{5/6}$□$_{1/6}I_2$)$^{1/3-}$]$_3$, which is entirely consistent with the recurrent stabilization in such radical cation salts of one-electron oxidized mixed valence *π*-dimers. This description assumes that no charge is transferred between the redox, mixed valence *π*-dimers within the metallic organic slab and the semiconducting [Pb$_{5/6}$□$_{1/6}$I$_2$$^{1/3-}$] layer, a matter which has been the object of debate in the literature.[31−33]

***β*-(EDT-TTF-I$_2$)$_2$$^{\bullet+}$[(Pb$_{2/3+x}Ag_{1/3-2x}$□$_xI_2$)$^{1/3-}$]$_3$, *x* ≈ 0.05, 2.** The opportunity to fill the former vacancies and manipulate the electronic properties by alloying the metal site with a second metal, combined with reports of earlier attempts at doping PbI$_2$ crystals with AgI,[34,35] prompted our attempts at setting up electrocrystallization experiments in the presence of AgI dispersed in acetonitrile. Thus, high-quality single crystals of a novel, lead−silver alloy are readily grown at the electrode. Mixtures of the two phases have never been observed nor did the former lacunary phase **1** grow in the presence of Ag$^+$. At variance with the observation of equal amounts of vacancies (or metal atom) on each independent metal sites in **1**, the structure refinements (vide supra) conclude that the metal site in general position is fully occupied by one lead atom and the metal site on the inversion center contains 0.40(2) Pb and 0.52(2) Ag, that is, ca. 8% of this particular site being left unoccupied. This is entirely consistent with the EPMA data. Thus, assuming again a constant net negative charge for the inorganic slab and the stabilization of one-electron-oxidized *π*-dimers, also consistent with the similarity of the electronic band structures and transport properties of **1** and **2**, the EPMA data have ultimately served for the compound formulation, *β*-(EDT-TTF-I$_2$)$_2$$^{\bullet+}$[(Pb$_{2/3+x}Ag_{1/3-2x}$□$_xI_2$)$^{1/3-}$]$_3$, *x* ≈ 0.05.

Deciphering the Structures: Commensurate Molecular Interface. As exemplified in a view of a fragment of the organic−inorganic interface where truncated EDT-TTF-I$_2$ molecules are projected onto the surface of one Pb$_x$Ag$_y$I$_2$ slab (Figure 3a), the respective positions of the iodine atoms bonded to the organic molecules and the inorganic iodides at the apexes of the octahedra are such as to satisfy a quasi-hexagonal compact motif.

That is, the molecular slabs are positioned in such a way as to allow for the hybrid sequence described in Figure 3c to develop along *c*. Hence, the organic iodine atoms typically occupy the inorganic iodide sites of the vicinal slab in the structure of the simplest, common ...(A*γ*B)(A*γ*B)... *2H*-PbI$_2$ polytype shown in Figure 3b. The relevant, interfacial, and shortest organic iodine···inorganic iodide van der Waals separations amounts to I5···I2 = 4.09(13) Å and I5···I3 = 3.81(14) Å in *β*-(EDT-TTF-I$_2$)$_2$$^{\bullet+}$[(Pb$_{5/6}$□$_{1/6}I_2$)$^{1/3-}$]$_3$ and I5···I2 = 4.1371(9) Å and I5−I3 = 3.7176(10) Å in *β*-(EDT-TTF-I$_2$)$_2$$^{\bullet+}$[(Pb$_{2/3+x}Ag_{1/3-2x}$□$_xI_2$)$^{1/3-}$]$_3$, *x* ≈ 0.05 for a standard van der Waals cutoff of 4.0 Å (the atom numbering is given in the Supporting Information). The I···I separation across the van der Waals gap in *2H*-PbI$_2$ is about 4.95 Å.

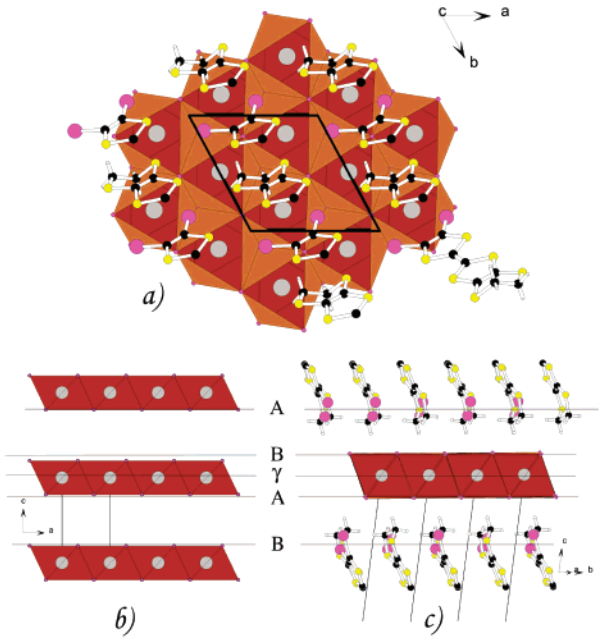

Figure 3. Two views, orthogonal to one another, of the organic−inorganic interface topology, exemplifying in both cases how the organic iodine atoms (purple) fit onto the metal iodide slabs: (a) note that only one organic molecule has been entirely drawn; (b) a representation of *2H*-PbI$_2$, described as a hexagonal compact ...ABAB... sequence of iodide with the metal atoms occupying one out of two octahedral sites (the so-called *γ*-sites) along *c*; (c) by analogy, the present hybrid intercalate interface topology shown in this representation may also be seen as a [.../moleculeA](B*γ*A)[Bmolecule/...] sequence, a consequence of the quasi-close-packing association of organic and inorganic iodine.

The single general position for the organic molecule is found only partially occupied in *β*-(EDT-TTF-I$_2$)$_2$$^{\bullet+}$[(Pb$_{5/6}$□$_{1/6}I_2$)$^{1/3-}$]$_3$. The remaining amounts of molecule are constrained by symmetry to be equally distributed on the translation-related positions labeled 2 and 3 in Scheme 2. The environment as seen from a molecule located on any of these three sites is identical providing that the two octahedra corresponding to the two independent lead atom sites are also identical. Refinement of the lead atom sites occupancy (gray and black sites in Scheme 2) concludes that the latter indeed contain the same amounts (16%) of lead and that the geometry of the octahedra is similar.

In the lead−silver alloy, there are different amounts of each of the two metals on the two independent sites and the octahedron associated with the silver-containing site is now somewhat distorted, with center-to-iodide distances ranging from 2.9105(9) to 3.3620(6) Å. It is therefore striking to observe that only one out of the three translation-related molecular sites is found to be fully occupied in the lead−silver alloy.

(32) (a) Ghorayeb, A. M.; Coleman, C. C.; Yoffe, A. D. *J. Phys C: Solid State Phys.* **1984**, *17*, L715−L719. (b) Coleman, C. C.; Magness, B.; Melo, P.; Goldwhite, H.; Tikkanen, W.; Tham, Q.; Pham, K.; Jacubinas, R.; Kaner, B.; Treece, R. E. *J. Phys. Chem. Solids* **1996**, *57* (6−8), 1153−1158.
(33) Warren, R. F.; Liang, W. Y. *J. Phys.: Condens. Matter* **1993**, *5*, 6407−6418.
(34) Jain, A.; Trigunayat, G. C. *Acta Crystallogr. A* **1996**, *52*, 590−595.
(35) Rush, G. E.; Chadwick, A. V.; Pannell, C. N.; Bilsborrow, R. L. *Radiat. Eff. Defects Solids* **1999**, *149*, 315−321.

Scheme 2

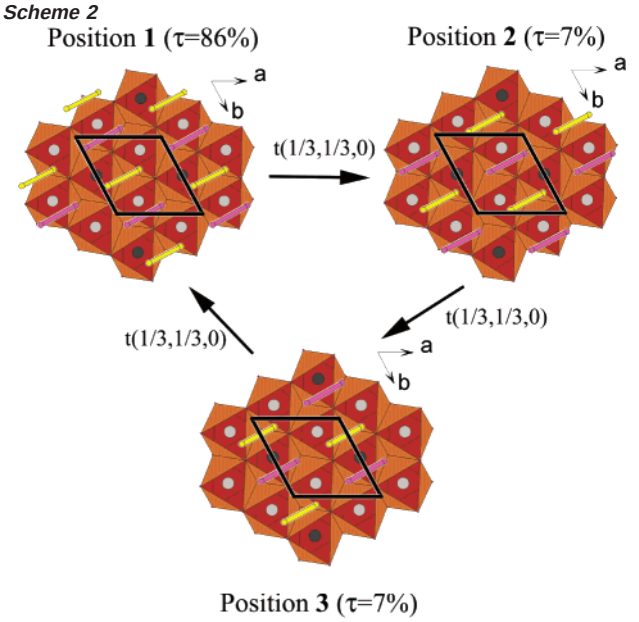

The grey (general position) and black (inversion center) dots differentiate the two independent crystallographic metal sites. The π-donor locations are symbolized by yellow (for those whose ethylenedithio ends reach out toward this particular inorganic slab) and purple (for those whose terminal iodines reach out toward this particular inorganic slab) lines. This scheme represents the three translation-related positions— labeled 1, 2, and 3—where the organic molecules are located, albeit with different net occupancies, in β-(EDT-TTF-I_2)$_2^{\bullet+}$[$(Pb_{5/6}\square_{1/6}I_2)^{1/3-}$]$_3$.

Table 2. S···S Distances Shorter than 4.0 Å and Absolute Values of the $\beta_{HOMO-HOMO}$ Interaction Energies (eV) for the Different Donor···Donor Interactions in β-(EDT-TTF-I_2)$_2^{\bullet+}$[$(Pb_{5/6}\square_{1/6}I_2)^{1/3-}$]$_3$ and β-(EDT-TTF-I_2)$_2^{\bullet+}$[$(Pb_{2/3+x}Ag_{1/3-2x}\square_xI_2)^{1/3-}$]$_3$, $x \approx 0.05$ (in Brackets)

interaction type[a]	S···S distances (Å)	$\beta_{HOMO-HOMO}$ (eV)
I	3.853[3.851] (×2), 3.861[3.858] (×2), 3.867[3.869] (×2)	0.3773 [0.3773]
II	3.698[3.717] (×2), 3.857[3.832] (×2), 3.873[3.860] (×2)	0.3680 [0.3732]
III	3.988[4.030][b]	0.0383 [0.0406]
IV	3.594[3.609] (×2), 3.597[3.957]	0.0091 [0.0142]
V	4.221[c][4.203][c]	0.0226 [0.0272]

[a] See Figure 4a for labeling. [b] The shortest S···S contact has been given. [c] The shortest S···S contact has been given. There are also short S···I contacts.

Intercalated β-Slabs with Quasi-One-Dimensional (1D) Electronic Structures and Charge Density Wave (CDW) Instabilities. A representation of the donor layers of the two salts approximately viewed along the long molecular axis is shown in Figure 4a. The layer can be seen as a series of parallel chains of donors along the *b*-direction arranged in a typical β-type way. Every molecule is engaged in intermolecular interactions with its six nearest neighbors: interactions I and II are intrachain interactions and interactions III−V are interchain interactions. The S···S distances shorter than 4.0 Å and the absolute values of the $\beta_{HOMO-HOMO}$ interaction energies associated with the five different intermolecular interactions of the β-(EDT-TTF-I_2)$_2^{\bullet+}$[$(Pb_{5/6}\square_{1/6}I_2)^{1/3-}$]$_3$ and β-(EDT-TTF-I_2)$_2^{\bullet+}$-[$(Pb_{2/3+x}Ag_{1/3-2x}\square_xI_2)^{1/3-}$]$_3$ salts are reported in Table 2.

It is quite clear from the values of this table that the donor layers of the two salts are very similar both structurally and electronically so that from now on only the results for the first salt will be discussed. The values of the $\beta_{HOMO-HOMO}$ interaction

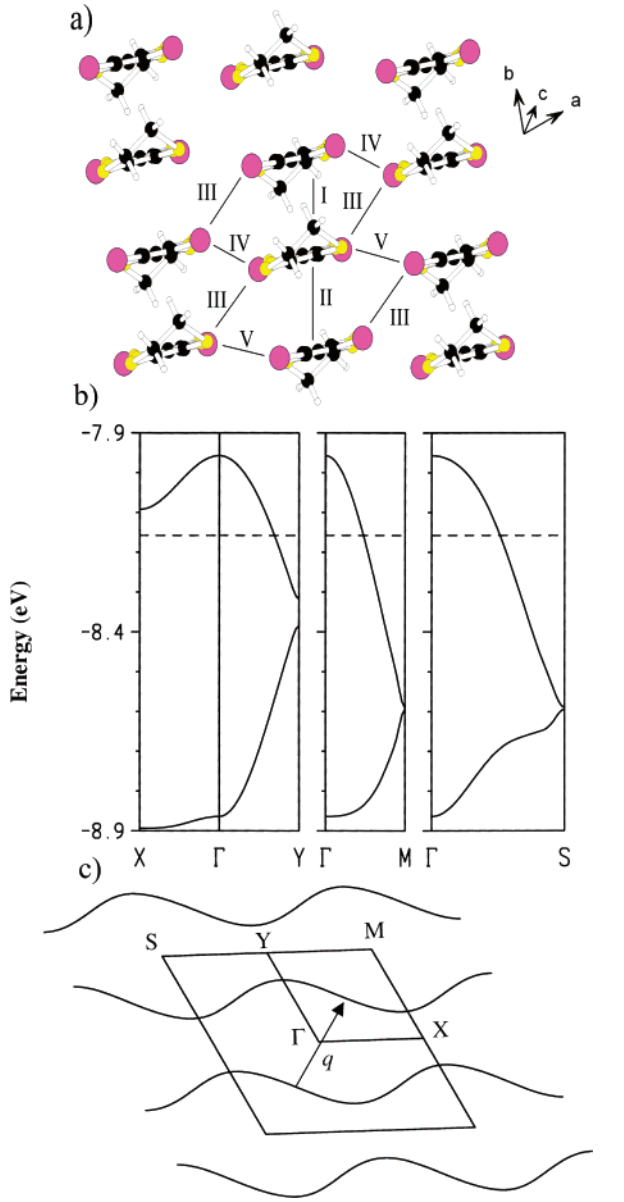

Figure 4. (a) Donor layer of β-(EDT-TTF-I_2)$_2^{\bullet+}$[$(Pb_{5/6}\square_{1/6}I_2)^{1/3-}$]$_3$ viewed approximately along the long molecular axis where the five different types of intermolecular interactions are labeled; (b) Calculated band structure for a donor layer of β-(EDT-TTF-I_2)$_2^{\bullet+}$[$(Pb_{5/6}\square_{1/6}I_2)^{1/3-}$]$_3$. The dashed line refers to the Fermi level and $\Gamma = (0, 0)$, $X = (a^*/2, 0)$, $Y = (0, b^*/2)$, $M = (a^*/2, b^*/2)$, and $S = (-a^*/2, b^*/2)$; (c) Fermi surface associated with the band structure in (b) where the nesting vector $q = 1/2(a^* + b^*)$ is indicated.

energies are noticeably different from those of typical β-type salts such as for instance those of the β-(BEDT-TTF)$_2$X (X = IBr_2, I_3, AuI_2, etc.) series of superconductors.[36] In the salts of this family, the two different intrachain interactions (I and II) differ by as much as a 30% (i.e., 0.287 and 0.439 eV for β-(BEDT-TTF)$_2I_3$ calculated with the same computational details as the results of Table 2) so that the chains are better seen as chains of dimers. In contrast, the interactions along the chains of the present salts are very uniform. In addition, one of the interchain interactions in the β-(BEDT-TTF)$_2$X series (0.024, 0.164, and 0.066 eV in β-(BEDT-TTF)$_2I_3$) is considerably stronger than here (see interactions III−V in Table 2).

(36) Whangbo, M.-H.; Williams, J. M.; Leung, P. C. W.; Beno, M. A.; Emge, T. J.; Wang, H. H. *Inorg. Chem.* **1985**, *24*, 3500−3502.

The two features, uniform interactions along the chains and smaller interchain interactions, should confer a pseudo-1D electronic structure to the present salts, in contrast with the typical two-dimensional one of the β-(BEDT-TTF)$_2$X family.[37] The difference can be traced back to the different type of chains. Whereas they exhibit a zigzag arrangement in the β-(BEDT-TTF)$_2$X family, in the present salts every successive pair of donors are arranged in a head-to-tail way resulting in an almost uniform shift along the same direction of the central C═C bond of adjacent donors of the chain. This arrangement is a consequence of the asymmetric nature of the donor and the willingness to establish I···H−C hydrogen bonds along the chains.

The calculated band structure of Figure 4b is in excellent agreement with the qualitative analysis. The two HOMO bands of Figure 4b exhibit a small dimerization gap (at Y) and a marked difference in dispersion along the a^* (Γ→X) and b^* (Γ→Y) directions. Because of the stoichiometry, there are three electrons to fill the two quite dispersive HOMO bands and, consequently, the salts are predicted to be metallic. The calculated Fermi surface (see Figure 4c) exhibits two warped lines running along the a^*-direction as expected for a pseudo-1D metal with better conductivity along the chains direction. The more interesting feature of this Fermi surface is the existence of the nesting vector $q = 1/2(a^* + b^*)$ (see Figure 4c) which allows a complete superposition of the two warped lines. This suggests the possibility of a CDW Fermi surface instability leading to a structural modulation with this wave vector. This would completely destroy the Fermi surface so that the resistivity versus temperature curve would exhibit a metal-to-insulator transition.[38] What is the physical meaning of this nesting vector? The warped lines of the Fermi surface are perpendicular to the b-direction which is the direction along which the donors pile up. Given the 1D character of the Fermi surface, the b^* component of q corresponds to the $2k_F$ wave vector.[39] Since the repeat unit of the stack contains two donors and the total charge transfer is given by $4k_F$, its value (1/2) corresponds to the charge transfer per donor molecule. It also leads directly to the new periodicity of the modulated phase along the b-direction, which is given by the inverse of this component (i.e., there would be a doubling of the periodicity). The $a^*/2$ component of q means that the CDW modulations will be out-of-phase in successive chains of the layers and consequently the new unit cell will also be twice along the a-direction.

Metals with a Metal−Insulator Transition at 70 K. As shown in Figure 5 and in agreement with the former analysis of their electronic band structures, both phases are metallic with room-temperature conductivity of 2.5 S cm^{-1} and 110 S cm^{-1} for **1** and **2**, respectively. The magnetic susceptibility, measured for **1** only, is essentially constant down to low temperature, as expected for a metal, and amounts to 9 10^{-4} emu·mole^{-1}, a value typical of organic metals. The EPR spectra for polycrystalline samples of **1** and **2** exhibit one single resonance centered at a g value of 2.007 with a line width $\Delta H = 150$ G, typical for pi-electron spins.[40] These data provide strong additional evidence that the metallic character arises from the organic layers only, typically with no contribution from the inorganic slabs.

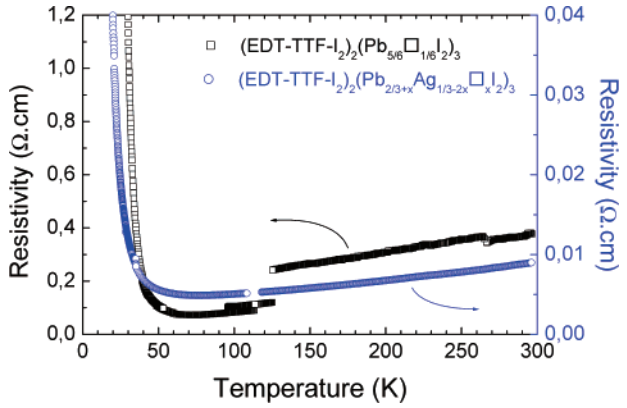

Figure 5. Temperature dependence of the resistivity for **1** and **2** measured in each case on one single crystal. The discontinuity of the resistivity data for β-(EDT-TTF-I$_2$)$_2$[(Pb$_{5/6}$□$_{1/6}$I$_2$)]$_3$ (squares) is the manifestation of the occurrence of tiny breaks within the single crystal upon slow cooling.

The two salts undergo a metal-to-insulator transition around 70 K and display semiconducting behaviors at low temperatures with activation energy of 200 and 80 K for **1** and **2**, respectively. The organic conducting layers are sandwiched between inorganic slabs of different compositions and therefore experience different electrostatic environments. This may affect their conductivity and gap value. In principle, the loss of the metallic properties could originate from a structural (i.e., the CDW instability) or an electronic localization mechanism. However, the rather abrupt change in the conductivity regime as well as the fact that the change occurs at almost the same temperature despite the differences in the anion layers, strongly suggest that the metal-to-insulator transition is associated with the CDW mechanism. In addition, let us note that the transverse component ($a^*/2$) of the nesting vector, by leading to out-of-phase modulations in successive chains, also leads to a minimization of the interchain coulomb interactions, and thus, the driving force for the structural modulation would be quite strong. Definite proof for this scenario could be obtained through the observation of superlattice spots at $1/2(a^* + b^*)$ in X-ray diffuse scattering experiments.[39] As discussed above, the b^* component of these superlattice spots is a measure of the band filling and thus gives relevant information concerning the Pb deficiency.

Conclusion

The synthesis of single crystals of β-(EDT-TTF-I$_2$)$_2^{\bullet+}$-[(Pb$_{5/6}$□$_{1/6}$I$_2$)$^{1/3-}$]$_3$ and β-(EDT-TTF-I$_2$)$_2^{\bullet+}$[(Pb$_{2/3+x}$Ag$_{1/3-2x}$□$_x$-I$_2$)$^{1/3-}$]$_3$, $x \approx 0.05$, and resolution of their complex structures, which include a state-of-the-art, combined microprobe and structural analysis of the metal sites vacancies/occupancies patterns, allow for a comparison of the topologies of this unique set of two complementary interfaces and reveal that the organic molecules are not strained upon anchoring on the PbI$_2$ slabs. At the organic−inorganic interface, a complementary, commensurate pattern of association is revealed instead where the organic iodine atoms typically occupy the inorganic iodide sites of the vicinal slab in the structure of the simplest, common *2H*-

(37) Whangbo, M.-H.; Williams, J. M.; Leung, W. P. C.; Beno, M. A.; Emge, T. J.; Wang, H. H.; Carlson, K. D.; Crabtree, G. W. *J. Am. Chem. Soc.* **1985**, *107*, 5815−5816.
(38) (a) Canadell, E.; Whangbo, M.-H. *Chem. Rev.* **1991**, *91*, 965−1034. (b) Jérome, D.; Schulz, H. J. *Adv. Phys.* **1982**, *31*, 299−490.
(39) Moret, R.; Pouget, J. P. In *Crystal Chemistry and Properties of Materials with Quasi-One-Dimensional Structures*; Rouxel, J., Ed.; Reidel: Dordrecht, The Netherlands, 1986, 87−134.
(40) Sugano, T.; Saito, G.; Kinoshita, M. *Phys. Rev. B: Condens. Matter* **1986**, *34*, 117−125.

PbI_2 polytype. Altogether the structural study reported herein represents the first single-crystal structure resolutions of any lead iodide phase with the CdI_2 structure type as well as of any layered PbI_2 intercalation compound.

Attempts at provoking similar single crystalline associations by engaging similar, albeit nonfunctional π-donors, such as TTF, EDT-TTF, and BEDT-TTF have consistently failed which is taken as an indication of the robustness of our rational-design approach aiming at directing the construction of a complementary interface by manipulating I···I van der Waals interactions.

A remarkable outcome of this work is the conservation of the electronic structure, room-temperature metallic character, and metal−insulator transition of the two-dimensional organic slabs upon alloying of the inorganic sublattice with monocations. However, the room-temperature conductivity of the lead−silver alloy is 2 orders of magnitude larger than that of β-(EDT-$TTFI_2)_2^{\bullet+}[(Pb_{5/6}\square_{1/6}I_2)^{1/3-}]_3$. A more thorough understanding of the role of the mixed-metal alloying of the inorganic sub-slabs on the metallic state in these series calls for the study of materials with diverse alloying patterns with metal cations of different nature and charges. These studies are currently under way.

Acknowledgment. This work was supported by DGI-Spain (Project BFM2000-1312-C02-01), Generalitat de Catalunya (Project 2001 SGR 333), the French-Spanish Program CNRS-CSIC (20000-01/7944), and by the Ministère de l'Education Nationale (France) (Ph.D grant to T. D.). We thank Marcel Bohn, IFREMER Brest (France) for EPMA measurements and Philippe Molinié, Institut des Matériaux Jean Rouxel, France, for his support in performing the ESR measurements.

Supporting Information Available: Tables of electron probe microanalysis data, experimental crystallographic details, tables of positional and thermal parameters, and additional crystallographic data (CIF). This material is available free of charge via the Internet at http://pubs.acs.org.

JA0290431